QUASI-ELASTIC LIGHT-SCATTERING SPECTRA OF SWIMMING SPERMATOZOA

ROTATIONAL AND TRANSLATIONAL EFFECTS

T. CRAIG, F. R. HALLETT, AND B. NICKEL, *Department of Physics, University of Guelph, Guelph, Ontario N1G 2W1 Canada*

ABSTRACT The electric field autocorrelation functions of light scattered from normal swimming bull spermatozoa are shown to be dependent on the mean head rotation frequency and not on the translational speed of the cells, as previously believed. This result was obtained from numerical generation of functions in which spermatozoa were modeled as Rayleigh-Gans-Debye ellipsoids having semiaxes $a = 0.5$ μm, $b = 2.3$ μm, and $c = 9.0$ μm. The magnitude of c required to achieve agreement with the experimental data is larger than the half-length of the head region of the cell. This implies that the midpiece, which also lies along c, contributes to the scattering power. Details regarding swimming trajectory and head orientation are included in the model. Analyses of the calculated functions and comparisons with experimentally determined ones suggest that at a scattering angle of 15° the electric field autocorrelation function can be fit by a simple Lorentzian whose half-width is inversely proportional to the scattering vector and the mean head rotational frequency.

INTRODUCTION

The potential of quasi-elastic light-scattering techniques for studying the swimming motion of motile cells has been investigated by several groups (Hallett et al., 1978; Holz and Chen, 1978*a*). Many attempts at studying spermatozoal motility have been reported (Adam et al., 1969; Dubois et al., 1975; Cooke et al., 1976; Jouannet et al., 1977; Shimizu and Matsumoto, 1977; Hallett et al., 1978). All of the latter investigations interpreted either the measured autocorrelation functions or the measured frequency spectra on the basis of a theory introduced by Nossal (1971). This theory stated that the electric field autocorrelation function of the scattered light, $g^{(1)}(\tau)$, can be related to the swimming speed distribution function, $P_s(v)$, through the relation

$$g^{(1)}(\tau) = \int_0^\infty \frac{\sin(kv\tau)}{kv\tau} P_s(v)\, dv, \tag{1}$$

where k is the magnitude of the scattering vector and τ is the experimental delay time. With a judicious choice of the swimming speed distribution function (Hallett et al., 1978) the average swimming speeds determined using Eq. 1 are comparable with or perhaps slightly higher than those obtained by other methods, such as cinematography (Rikmenspoel, 1960). This success, coupled with the relatively short amounts of experimental and analysis time involved, could

---

Dr. Nickel is an Alfred P. Sloan Fellow.

allow the light-scattering technique to become a clinical and industrial tool for the rapid measurement of cellular viability.

The formulation of Eq. 1 rests, however, on two major assumptions: (*a*) that the scattering particles move in trajectories that are straight for times of the order of $(kv)^{-1}$ and (*b*) that the scattering particles behave as point scatterers. In most of the experiments to date on spermatozoa the minimum value of k has been $\sim 3.0\ \mu m^{-1}$. For normally swimming motile cells the typical speed along the helical trajectory is $\sim 300\ \mu m\ s^{-1}$. Since the cells require ~0.1 s to complete one turn of the helix, they progress $\sim 1/100$ of the cycle in the time $(kv)^{-1}$. On these grounds the first assumption appears reasonably good. It is unlikely, however, that a bull spermatozoon with an ellipsoidal head region measuring 1 μm × 4.6 μm × 9 μm (van Duijn and van Voorst, 1971), and with a long slender midpiece and tail can be reasonably approximated as a point scatterer. Recently, Chen et al. (1977) extended the theory by considering the scatterers as Rayleigh-Gans-Debye particles. They applied this extended theory to the case of motile *E. coli* bacteria, which they treated as coated prolate ($a > b = c$) ellipsoids. In a subsequent publication (Holz and Chen, 1978*b*) they included effects due to the rotational motion of these ellipsoids and found that the functions predicted by the theory were in good agreement with those obtained experimentally.

In this paper we report a similar investigation of the spermatozoon system. Electric field autocorrelation functions have been analytically determined for two model systems: spheroids with semiaxes $a < b = c$, and ellipsoids with semiaxes a, b, and c. The trajectories assumed for these model particles are based as closely as possible on the real helical trajectories exhibited by normal bull spermatozoa. To further model the real situation we include distribution functions for both the translational speeds and the head rotation frequencies. Good agreement with experimental functions is found when entire spermatozoa are modeled as ellipsoids with the semiaxes 0.5 μm × 2.3 μm × 9.0 μm having average rotational frequencies of 10.0 Hz. The value 2 × 9.0 μm corresponds to a distance equal to the length of the head plus about two-thirds of the midpiece of the cell. The other two values of the semiaxis are those mentioned earlier for the head alone. The calculations indicate that for a particle of this shape the mean head rotation frequency is the dominant factor determining the half-width at half-height of the calculated functions. The effect of translational motion is very small. We can understand these results qualitatively in the following manner.

What one observes in a light-scattering experiment is a superposition of scattered amplitudes. The observed decay of correlations occurs as a result of a loss, or more specifically a change, in the phase coherence of the scattered waves. In point scatterers this loss of coherence occurs on a time scale given by the time it takes a typical particle to move a half "wavelength" πk^{-1}. That is, for point scatterers, the correlation time $\tau \simeq \pi(kv)^{-1}$, where v is a typical speed parallel to k and is not much different from the mean speed (cf. Eq. 1).

At the other extreme of large disk-like objects with a typical linear dimension ℓ, one observes predominantly those particles for which the normal to the disk and $\mathbf{k}$ lie within the diffraction cone, i.e., within an angle $\delta\theta \simeq 2\pi(k\ell)^{-1}$. If the disk motion is parallel to the disk face, then the decay time for correlations due to the translational motion is greatly increased because one sees predominantly those particles that move perpendicular to $\mathbf{k}$. The typical speed parallel to $\mathbf{k}$ is now only $\simeq v\delta\theta$, so that the decay time $\tau_{trans} \simeq \pi(kv\delta\theta)^{-1} \simeq \ell(2v)^{-1}$. However, if the disks rotate about an axis parallel to the disk face there exists a second

mechanism for loss of coherence. That is, the coherence will change on a time scale given by the time it takes the normal to the disk to sweep through the diffraction cone. This rotational correlation time is: $\tau_{rot} \simeq \delta\theta/\omega \simeq 2\pi(k\ell\omega)^{-1}$. For example, choosing $\ell = 10$ μm, $v = 300$ μm s^{-1}, $\omega = 60$ s^{-1}, and $k = 3$ μm^{-1}, we obtain $\tau \simeq \tau(kv)^{-1} \simeq 3$ ms for points, whereas we obtain $\tau_{trans} \simeq \ell(2v)^{-1} \simeq 20$ ms, $\tau_{rot} \simeq 2\pi(k\ell\omega)^{-1} \simeq 3$ ms for disks. Clearly we observe only rotations and it is the accidental near equality of v for points and $\ell\omega$ for large disks that has led to the previous misinterpretations of the experimental data.

THEORY

In the following discussion we consider an ellipsoidal Rayleigh-Gans-Debye particle of semiaxes *a, b,* and *c* progressing along a helical trajectory such that the a semiaxis continually intersects the axis of the helix (Fig. 1). A similar treatment of a prolate spheroid rotating about an axis that may or may not coincide with an axis through its center of mass has been given by Holz and Chen (1978*b*). In our model the electric field autocorrelation function can be written as

$$g^{(1)}(\tau) = C_N^{-1}\left\langle \frac{1}{4\pi}\int_0^{2\pi} d\psi_0 \int_{-1}^{1} d\nu\, e^{ikv\nu\tau}\, e^{i\mathbf{k}\cdot[\mathbf{R}(\tau)-\mathbf{R}(0)]} \cdot A(\mathbf{k},\tau)\, A^*(\mathbf{k},0)\right\rangle, \qquad (2)$$

where C_N is a normalization factor, τ is a delay time, and $\mathbf{R}(\tau)$ is the component of the instantaneous position of the scatterer perpendicular to the axis of the helix. Eq. 2 assumes that the motion of the particle is straight for a time $(kv)^{-1}$, an assumption which was justified earlier. The form factor $A(\mathbf{k},\tau)$ is the instantaneous scattering amplitude of the particle determined by its overall shape and orientation with respect to the scattering vector **k**. The integrations in Eq. 2 average the autocorrelation over $\nu = \cos\theta$, the projection of $\mathbf{k}/k$ on the axis of the helix, and over the azimuthal angle ψ_o, which specifies the position of the scatterer at $\tau = 0$. The brackets $\langle\ \rangle$ indicate additional averaging over characteristics of the motion such as the progressive swimming speed v.

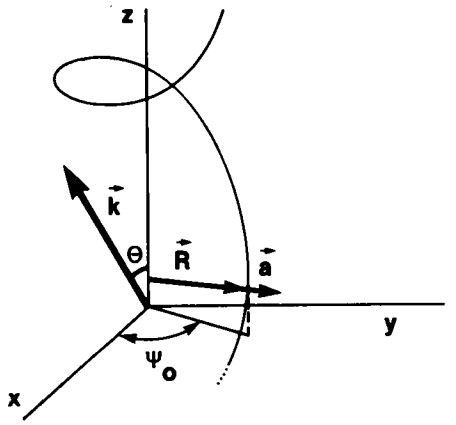

FIGURE 1 The helix frame showing the direction of motion, *z*, the orientation of the scattering vector, **k**, the position vector, **R**, and the direction of one of the semiaxes, **a**.

The form factor has been evaluated by Chen et al. (1977) for coated spheroids. For the low angle (<20°) scattering of interest here the coating is probably not observable and has been neglected. On the other hand, a spermatozoon is not well described by an ellipsoid of revolution and we need the form factor given by

$$A(k,\tau) = \frac{1}{\frac{4}{3}\pi abc} \int_{\frac{\alpha^2}{a^2}+\frac{\beta^2}{c^2}+\frac{\gamma^2}{c^2}\le 1} e^{ik_a\alpha + ik_b\beta + ik_c\gamma}\, d\alpha d\beta d\gamma \tag{3}$$

where **a**, **b**, and **c** are the semiaxes of the ellipsoid. Writing $\alpha/a = \alpha'$, $\beta/b = \beta'$, and $\gamma/c = \gamma'$ yields

$$A(k,\tau) = \frac{3}{4\pi} \int_{\alpha'^2+\beta'^2+\gamma'^2\le 1} e^{iak_a\alpha' + ibk_b\beta' + ick_c\gamma'}\, d\alpha' d\beta' d\gamma' \tag{4}$$

which is the form factor of a sphere with scattering vector $(ak_a, bk_b, ck_c) = (\mathbf{k}\cdot\mathbf{a}, \mathbf{k}\cdot\mathbf{b}, \mathbf{k}\cdot\mathbf{c})$. Hence

$$A(\mathbf{k},\tau) = 3\, j_1(\kappa)/\kappa, \tag{5}$$

where

$$\kappa^2 = (\mathbf{k}\cdot\mathbf{a})^2 + (\mathbf{k}\cdot\mathbf{b})^2 + (\mathbf{k}\cdot\mathbf{c})^2 \tag{6}$$

and j_1 is the spherical Bessel function of order 1.

Since most of the mass of a spermatozoon is located in or near the head region the scattering power of the cell should be concentrated in this region as well. Fig. 1 shows the model we have chosen to represent the head motion while the cell is swimming normally. The coordinate system x, y, z is arranged such that the average direction of motion of the center of mass is along z. Furthermore, we choose the orientation of the coordinate system so that **k** lies in the xz plane. The centroid of the ellipsoid travels on a helical path of radius R. If we let ψ represent the instantaneous angle between **R** and the xz plane, then we take as our model

$$\psi = \psi(\tau) = \omega\tau + \psi_0, \tag{7}$$

where ω is the head rotation frequency and ψ_0 is the (random) position of the particle at $\tau = 0$, as shown in Fig. 1.

To represent the head orientations observed by time-lapse photography and cinematography, it is necessary to tilt the ellipsoid with respect to the overall direction of motion (z). This can be accomplished by first tipping the **a** axis downward by an angle β from the direction of **R**. This yields the "duck-footed" pattern observed photographically. The ellipsoid is then rotated by the angle α about the new direction of **a**. If β were zero a rotation $\alpha = \tan^{-1}(R\omega/v)$ would set **c** parallel to the helical trajectory of the centroid. The angles α and β are shown in Fig. 2. Values of $\alpha = 57°$ and $\beta = 12°$ were obtained in our own laboratory from analysis of about 20 tracks on time-lapse photographs.

The dot products required for the evaluation of the autocorrelation in Eq. 2 are

$$\mathbf{k}\cdot\mathbf{R} = Rk(\cos\psi \sin\theta) \tag{8a}$$

$$\mathbf{k}\cdot\mathbf{a} = ak(\cos\beta \cos\psi \sin\theta - \sin\beta \cos\theta) \tag{8b}$$

$$\mathbf{k} \cdot \mathbf{b} = -bk[(\cos\alpha \sin\psi + \sin\alpha \sin\beta \cos\psi)\sin\theta + \sin\alpha \cos\beta \cos\theta] \tag{8c}$$

$$\mathbf{k} \cdot \mathbf{c} = ck[(-\sin\alpha \sin\psi + \cos\alpha \sin\beta \cos\psi)\sin\theta + \cos\alpha \cos\beta \cos\theta]. \tag{8d}$$

Since the factor $e^{i\mathbf{k}\cdot\mathbf{R}(\tau)}\, A(\mathbf{k}, \tau)$ is periodic in the variable ψ we define

$$B(\mathbf{k}, \tau) = e^{i\mathbf{k}\cdot\mathbf{R}(\tau)}\, A(\mathbf{k}, \tau) = \sum_n B_n\, e^{in\psi}, \tag{9}$$

where the Fourier coefficients are

$$B_n = \frac{1}{2\pi} \int \mathrm{d}\psi\, e^{-in\psi}\, e^{i\mathbf{k}\cdot\mathbf{R}(\tau)}\, A(\mathbf{k}, \tau) \tag{10}$$

and depend on α, β, and θ and the dimensionless products Rk, ak, bk, and ck. A useful symmetry property with respect to $\nu = \cos\theta$ is

$$B_n(-\nu) = (-1)^n\, B^*_{-n}(\nu). \tag{11}$$

Since ψ is simply related to ψ_0 by Eq. 7 we obtain

$$\int \mathrm{d}\psi_0\, B(\mathbf{k}, \tau)\, B^*(\mathbf{k}, 0) = \sum_{nm} \int \mathrm{d}\psi_0\, B_n\, e^{in(\omega\tau + \psi_0)}\, B^*_m\, e^{-im\psi_0}$$

$$= 2\pi \sum_n |B_n|^2\, e^{in\omega\tau} \tag{12}$$

and hence

$$g^{(1)}(\tau) = C_N^{-1} \left\langle \frac{1}{2} \int_{-1}^{1} \mathrm{d}\nu\, e^{ik\nu\nu\tau} \sum_n |B_n|^2\, e^{in\omega\tau} \right\rangle$$

$$= C_N^{-1} \left\langle R \int_0^1 \mathrm{d}\nu\, e^{ik\nu\nu\tau} \sum_n |B_n|^2\, e^{in\omega\tau} \right\rangle, \tag{13}$$

where R denotes real part. This last equality in Eq. 13 can be verified with the use of the symmetry relation (Eq. 11). The various averages remaining in Eq. 13 are discussed below.

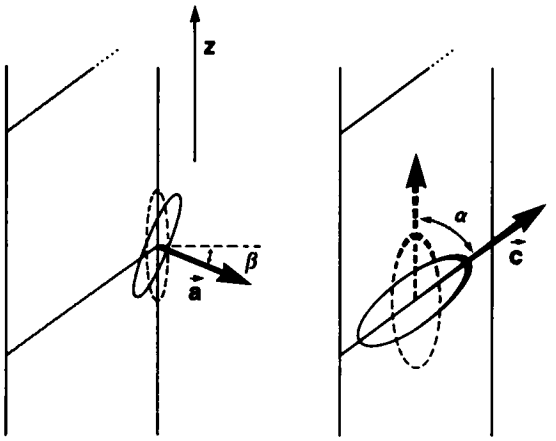

FIGURE 2 The tilt angles α and β shown with respect to the direction of motion and the helical trajectory. If shown, the midpiece and tail regions of the spermatozoa would lie along c.

Previous evidence (Jouannet et al., 1977; Hallett et al., 1978) suggested that the swimming speed distribution function for spermatozoa has the form

$$P_s(v) = \frac{4}{\bar{v}^2} e^{-2v/\bar{v}}. \tag{14}$$

If we average Eq. 13 over the distribution (14) we obtain

$$g^{(1)}(\tau) = C_N^{-1} R \int_0^1 d\nu (1 + iq_\nu)^{-2} \sum_n |B_n|^2 e^{in\omega\tau} \tag{15}$$

where

$$q_\nu = \frac{1}{2} k\nu\bar{v}\tau. \tag{16}$$

Eq. 15 has been used to predict the electric field autocorrelation functions from normal motile spermatozoa and some of these functions are shown in the following results session (Fig. 4). These functions exhibit severe oscillations not observed in the experimental functions. The difficulty here has arisen because in a real sample a distribution of head rotation frequencies occurs. Thus we have found it necessary to integrate over a head frequency distribution function as well. Since Rikmenspoel (1960) has demonstrated that the progressive speed and the head rotation frequency are linearly related, we have chosen a distribution function for the head rotation frequencies similar to the function (Eq. 14) used for speeds, namely

$$P(\omega) = \frac{4\omega}{\bar{\omega}^2} e^{-2\omega/\bar{\omega}}. \tag{17}$$

The choice of this particular distribution is further confirmed in the results section, where it is demonstrated that a normal distribution leads to functions that compare less well with the experimental ones. The result of averaging Eq. 15 over the distribution (Eq. 17) is

$$g^{(1)}(\tau) = C_N^{-1} R \int_0^1 d\nu \sum_n (1 + iq_\nu)^{-2} (1 + ip_n)^{-2} |B_n|^2 \tag{18}$$

where

$$p_n = \frac{1}{2} n\bar{\omega}\tau. \tag{19}$$

Note that in deriving Eq. 18 we have allowed v and ω to vary independently and hence that we have assumed the linear relationship shown by Rikmenspoel (1960) applies only to means; i.e., $\bar{v} = \xi\bar{\omega}$. An alternative interpretation of the data is that $v = \xi\omega$ for all ω. In this case Eq. 13 must be averaged over Eq. 14 only and the frequency constraint substituted into the integrand. We obtain

$$g^{(1)}(\tau) = C_N^{-1} R \int_0^1 d\nu \sum_n [1 + i(q_\nu + p_n)]^{-2} |B_n|^2, \tag{20}$$

where now

$$v = \xi \omega \tag{21}$$

and q_n and p_n are given as before by Eqs. 16 and 19. Although the correct model for normally swimming spermatozoa presumably lies somewhere between the complete independence or dependence of v and ω discussed above, the differences we observe in the functions generated by Eqs. 18 and 20 are small. Thus we have not investigated more complicated relationships or averaging procedures.

EXPERIMENTAL AND NUMERICAL METHODS

The details regarding the collection and handling of the bull spermatozoa samples as well as the spectroscopic techniques used have been described previously (Hallett et al., 1978). Most of the experimental autocorrelation functions used in the present study were described in that publication. The scattering angle employed in all these experiments was 15°. Since our intent was to compare predicted and experimental functions we deliberately chose an experimental function from a sample which by microscopic inspection contained few dead cells and no defective swimmers. This data and four others from similar samples could be extremely well fit with a sum of two functions: a Lorentzian function (f_N) for the normal swimmers, and a slowly decaying polynomial function (f_d) for the dead cells. The function f_d was determined from a separate experiment in which dead cells alone were examined. One of these experimental functions and the best-fit functions f_N and f_d are shown in Fig. 3. The function f_N was the best simple function for fitting the scattering function from normal cells in all 88 semen samples studied. The sample-to-sample variability in the half-width of f_N was typically

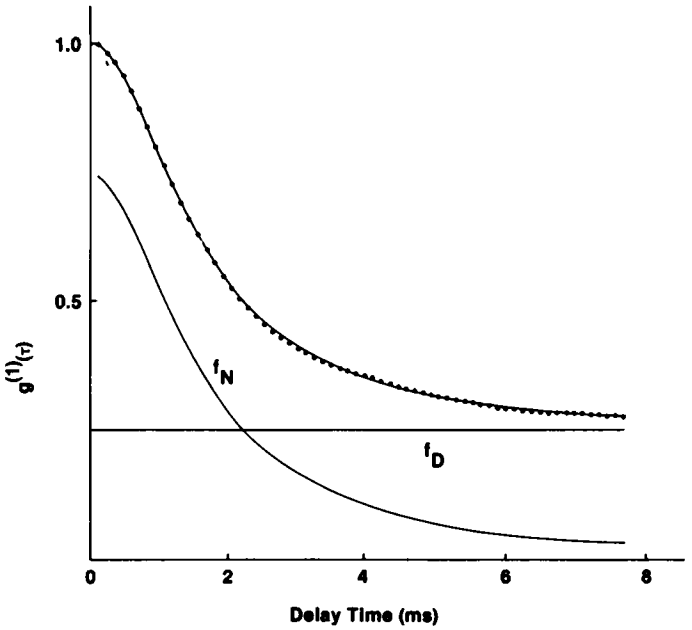

FIGURE 3 Best-fit functions, f_N, (a Lorentzian) and f_d (an experimentally determined polynomial) to an experimentally determined electric field autocorrelation function (dots) from bull spermatozoa. (Scattering angle = 15°).

<25%. The following results section contains a comparison between the best-fit function f_N, which has been normalized to unity at $\tau = 0$, and functions which have been generated using Eqs. 15, 18, and 20.

The numerical integrations in these equations were performed on a Nova-2 minicomputer (Data General Corp., Southboro, Mass.) containing 32K of memory and a real time disk operating system. Typically the generation of a 64-point scattering function required about 10–15 min of computer time. The Fourier coefficients, Eq. 10, were obtained by a fast-Fourier-transform routine and considerable economy of time was achieved by storing the form factor, Eq. 5, in a linear array and using an interpolation method to get function values for specific arguments. For values of the product ck of the order of 20 or less, 64 Fourier coefficients were found to be adequate; some of the larger values of ck treated here required 128 coefficients. The integral over ν was obtained by a Simpson's rule with 50 segments. This was found to give results accurate to at least four digits.

Time-lapse photographs of the swimming motion of the bull spermatozoa were taken using a standard 35-mm camera back mounted to a Zeiss microscope (Carl Zeiss, Inc., New York; Model KL14), equipped for dark-field viewing.

RESULTS

In the initial calculations the model representing the swimming spermatozoa was simplified as much as possible. This allowed us to gradually include effects due to shape change, trajectory change, and head tilt and to monitor the effects of each change. Thus, the cells were initially modeled as disks of half-thickness $a = 0.5$ μm and $b = c = 3.5$ μm. This compares to actual dimensions of the head region of a bull spermatozoon which are $a = 0.5$ μm, $b = 2.3$ μm and $c = 4.5$μm (van Duijn and van Voorst, 1971). In addition **R**, α, and β were set equal to zero. The disk faces remain parallel to the straightline motion along z. The normalized experimental scattering function f_N (solid line) is plotted in Fig. 4 with one function (dots) generated using Eq. 15. The average speed, and the single head rotational frequency were 300 μm s^{-1} and 20 Hz, respectively. These values were one set that yielded a function whose half-width matched the experimental function. However, the severe oscillations present in the generated

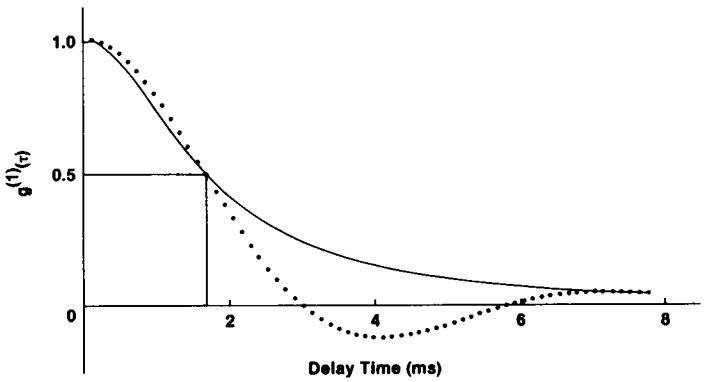

FIGURE 4 A comparison of f_N, a Lorentzian that represents the experimentally obtained scattering function (solid line), with a predicted scattering function calculated numerically from Eq. 15 (dots) using $\bar{v} = 300$ μm s^{-1}, $f = 20$ Hz, $a = 0.5$ μm, and $b = c = 3.5$ μm.

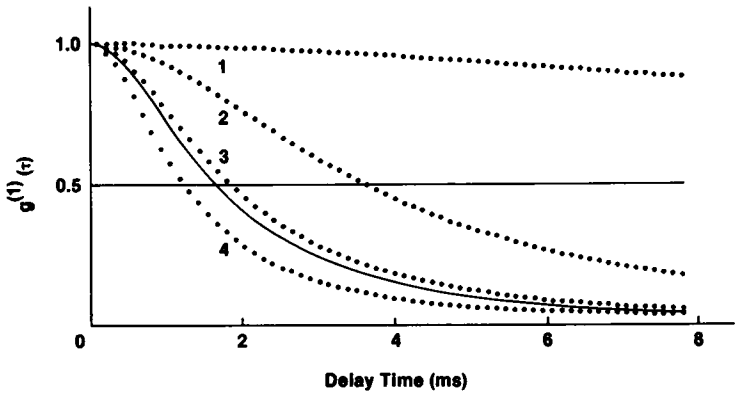

FIGURE 5 Scattering functions calculated numerically from Eq. 18 using $\bar{v} = 110\ \mu m\ s^{-1}$, $a = 0.5\ \mu m$, $b = c = 3.5\ \mu m$, $\bar{f}(1) = 0$ Hz, $\bar{f}(2) = 10$ Hz, $\bar{f}(3) = 20$ Hz, and $\bar{f}(4) =$ Hz.

function make detailed comparison with f_N difficult. These oscillations were removed when a frequency distribution was used, as in Eq. 18 or 20. Functions generated using Eq. 18 are shown in Fig. 5 for the same disk as above and with **R**, α, and β still equal to zero. In this case, however, an average progressive speed of 110 $\mu m\ s^{-1}$ was used, a value which is comparable with that obtained by cinematographic studies of motile bull spermatozoa (Rikmenspoel et al., 1960). It is clear from this diagram that increases in the frequency of head rotation lead to

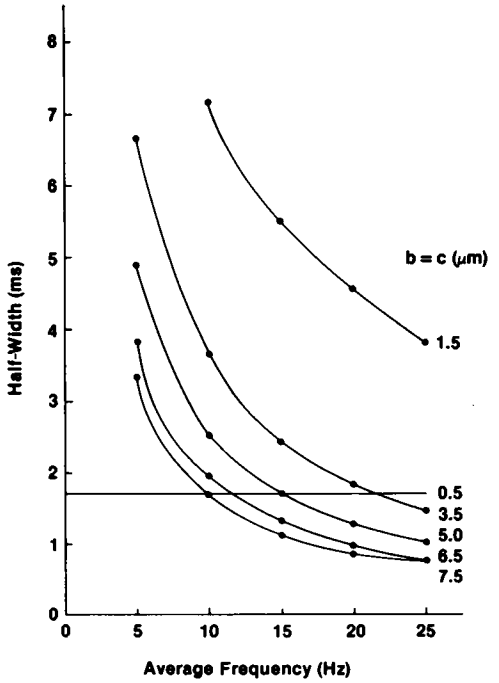

FIGURE 6 Half-width at half-height of the predicted scattering functions (using Eq. 18) as a function of mean head rotation frequency for disks having different axial ratios. ($a = 0.5$ m, $b = c$ values shown on graph). The average translational speed was 110 $\mu m\ s^{-1}$.

marked decreases in the decay times of the scattering functions. Comparison of the functions in Fig. 5 with f_N (solid line) indicates that a frequency of head rotation of ~25 Hz is required to make the decay times of the generated and experimental functions comparable. This is much higher than the cinematographically observed values of ~10 Hz (Rikmenspoel et al., 1960). For this reason we began a systematic investigation in which the half-width at half-height of the predicted function was determined as a function of both disk shape and rotational frequency. The results, summarized in Fig. 6, were obtained using Eq. 18 and inputting a fixed average speed of 110 μm s^{-1}. As the axial ratio increases the zero frequency width of the functions becomes enormous, an effect which has also been reported by Chen et al. (1977). However, even a small amount of head rotation quickly narrows the function; the larger the axial ratio, the more rapid the narrowing. If the particle shape is a sphere, the frequency dependence disappears and the width is determined solely by the translation speed (cf. $b = 0.5$ curve in Fig. 6). In other words, Eq. 2 collapses to Eq. 1 under these conditions.

We have recalculated the curves shown in Fig. 6 using a range of values for $\bar{v}$. It was apparent from these calculations that once the axial ratio of the effective scatterer has values greater than 3.5 μm:0.5 μm the half-width of the scattering function becomes independent of $\bar{v}$. This axial ratio dependent effect of velocity changes is illustrated in Fig. 7 in which average particle speed has been plotted against the head rotation frequency, which leads to a fixed half-width of 1.44 ms. The calculations have been repeated for several axial ratios. In the case of a sphere ($a = 0.5$ μm, $b = c = 0.5$ μm) the half-width corresponds to a $\bar{v}$ of 400 μm s^{-1}. Head rotation frequency is irrelevant in this case. In the curve for $a = 0.5$ μm, $b = c = 7.5$ μm, the opposite extreme occurs and the half-width is determined only by the average rotational frequency. Identical half-widths are obtained in this case if one inputs a v of 50 μm s^{-1} or a v of 400 μm s^{-1}. At an axial ratio of 3.5 μm:0.5 μm changes in particle speed have a small but noticeable effect and at 1.5 μm:0.5 μm the effects are sizeable. Thus it is clear that for motile disks having axial ratios greater than 7:1, the rotational motion becomes the dominant factor controlling the decay times of the scattering functions.

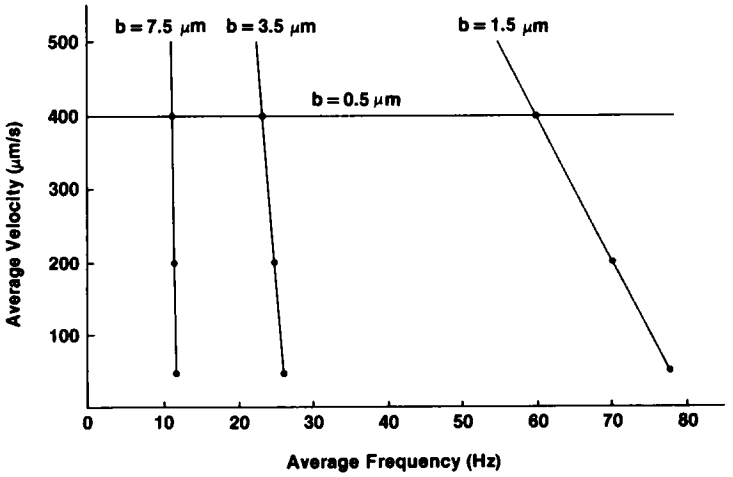

FIGURE 7 A figure showing the values of $\bar{v}$ and $\bar{f}$ required to produce predicted scattering functions that have a fixed half-width of 1.44 ms for disks. ($a = 0.5$ μm; $b = c$ values shown on graph).

The half-width at half-height of the experimental function, f_N, is 1.68 ms. If one chooses a mean head rotation frequency of ~10 Hz, based on cinematographic observations then according to the curves presented in Fig. 6, the disks must have an effective axial ratio on the order of 7.5 μm:0.5 μm to match this width. Fig. 8 shows a comparison between f_N (solid line) and a function calculated using an axial ratio of 7.5 μm:0.5 μm and a rotational frequency of 9.8 Hz (dots).

While the curves are clearly similar, the required disk-shape of $a = 0.5$ μm, $b = c = 7.5$ μm bears little resemblence to the actual head dimensions of $a = 0.5$ μm, $b = 2.3$ μm, $c = 4.5$ μm. Although such disks might be referred to as "equivalent" or "effective" disks, it would clearly be more useful if the model particle had dimensions closer to the real system. If the true head dimensions are utilized with no other changes to the model, then an increase in decay time is observed and one must use higher rotational frequencies again to obtain half-widths similar to f_N. This is because the model particle is forced to a straight line trajectory with tilt angles of zero ($R = 0$, $\alpha = 0$, $\beta = 0$). By increasing R one increases the helical character of the trajectory and by increasing α and β one changes the direction of the semiaxes of the ellipsoid with respect to the direction of motion (the z-axis). The effects of changes in these parameters on the shape and half-width of the scattering function were monitored. Changes in **R** produce no changes in the scattering function if the particle is sufficiently nonspherical that velocity changes are negligible. Increase in either α or β usually result in decreases in decay time. Any tilt or reorientation that displaces mass and hence scattering power from the axis of rotation of the particle tends to reduce the decay time. This effect is similar to increasing the $b = c$ semiaxes in the disk case described earlier.

Our approach in using these parameters was to use values for R, α, and β obtained from the analysis of tracks on photomicrographs ($R = 3.0$ μm, $\alpha = 57°$, $\beta = 12°$), and to fix $a = 0.5$ μm, $b = 2.3$ μm, $\bar{v} = 110$ μm s^{-1}, and $\bar{\omega} = 2\pi(10)s^{-1}$. The semiaxis c was adjusted until the half-width of the generated function matched the half-width of the experimental function f_N. As shown in Fig. 9, this occurs when c has a value of 9.0 μm. This value for c suggests that the scattering power of the spermatozoa is not due to scattering from the head region alone and

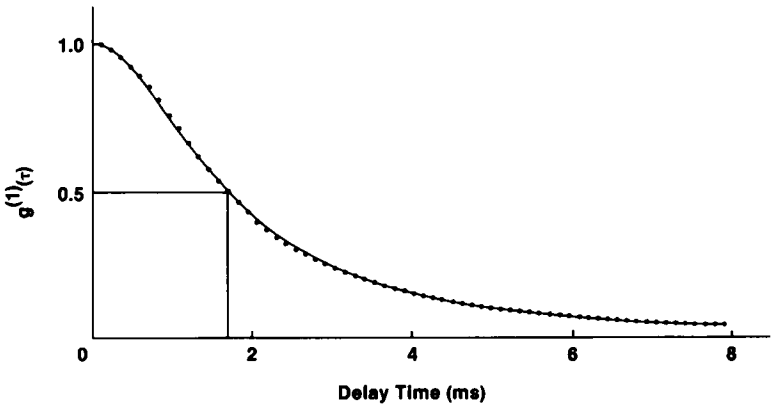

FIGURE 8 A comparison of f_N, a Lorentzian that represents the experimentally obtained scattering function (solid line), with a scattering function calculated using Eq. 18 and $\bar{f} = 10.0$ Hz, $a = 0.5$ μm, and $b = c = 7.5$ μm. The function is independent of the magnitude of $\bar{v}$.

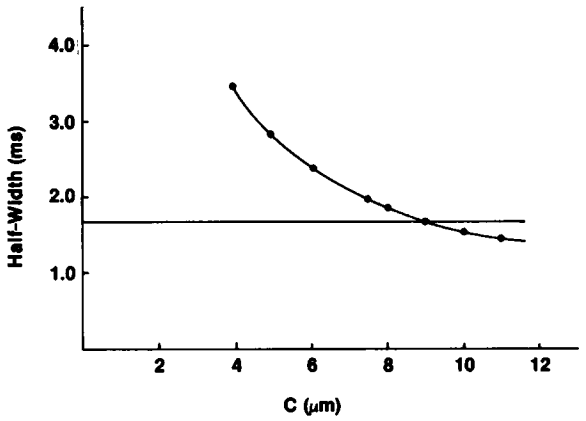

FIGURE 9 Half-widths of scattering functions determined as a function of c. (a = 0.5 μm, b = 2.3 μm, α = 57°, β = 12°, $\bar{f}$ = 10.0 Hz). This curve is unaffected by the magnitude of $\bar{v}$.

that the midpiece as well must be considered. A distance of 18 μm from the anterior end of the spermatozoa encompasses all of the head region of the spermatozoa and about two-thirds of the midpiece. It will be interesting to see if corresponding lengths can be used as a measure of the c-axis in other spermatozoal systems.

The function generated using Eq. 18 and the parameters described in the previous paragraph is compared with f_N in Fig. 10. The value of R was unimportant in this case; an identical function was generated using $R = 0$. Thus the ellipsoid having semiaxes a = 0.5 μm, b = 2.3 μm, and c = 9.0 μm is clearly in the regime where the translational speed of the particle can be neglected (changing R from 0 to 3.0 μm increases the center of mass speed by a factor of 2.13 for a helix of pitch equaling 10.0 μm).

Functions generated using Eq. 20 differ only marginally from ones generated using Eq. 18. A half-width of 1.68 ms now corresponds to a slightly higher c-value of 9.2 μm. This function is shown in Fig. 11. The first 20 points of the two functions (Figs. 10 and 11) are indistinguishable. Slight differences occur in the tail regions only. Although physically more

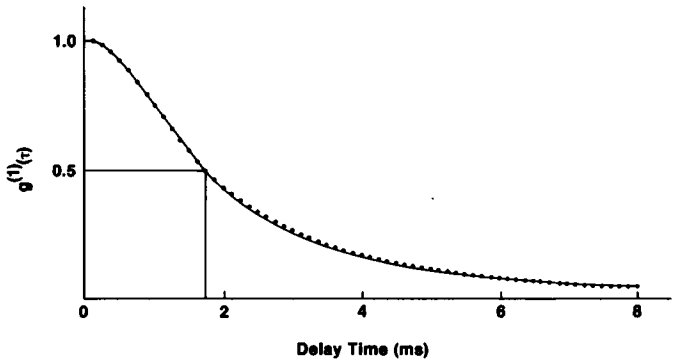

FIGURE 10 A comparison of f_N, a Lorentzian that represents the experimentally obtained scattering function (solid line) with a scattering function calculated using Eq. 18. (a = 0.5 μm, b = 2.3 μm, c = 9.0 μm, α = 57°, β = 12°, $\bar{f}$ = 10.0 Hz).

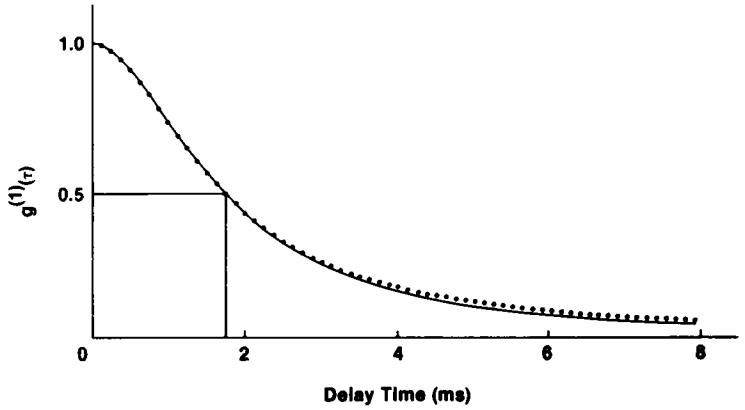

FIGURE 11 A comparison of f_N, a Lorentzian that represents the experimentally obtained scattering function (solid line) with a scattering function calculated using Eq. 20. (a = 0.5 μm, b = 2.3 μm, c = 9.0 μm, α = 57°, β = 12°, $\bar{f}$ = 10.0 Hz). This function is unaffected by the magnitude of $\bar{v}$.

likely, the function generated using Eq. 20 compares slightly less well with the function f_N. One reason may be that the coupling constant, ξ, between v and ω, is itself distributed; that is, a range of velocities may correspond to any one frequency. A more likely reason, however, relates to the assumption that the scattering function from normal swimmers can be approximated by a Lorentzian. While a Lorentzian is still the best simple function for this purpose, a more rigorous function, such as Eq. 20, would do equally well. However, prohibitive amounts of computing would be required for least squares fitting of Eq. 20 to experimental data. The few percent increases in accuracy that would be gained is certainly not worth the effort and expense involved.

It was also clear from the generation of several functions that other choices for the distribution function $P(\omega)$ gave less satisfactory results than the exponential distributions determined by Hallett et al. (1978) and used in Eqs. 18 and 20. For example, use of a normal

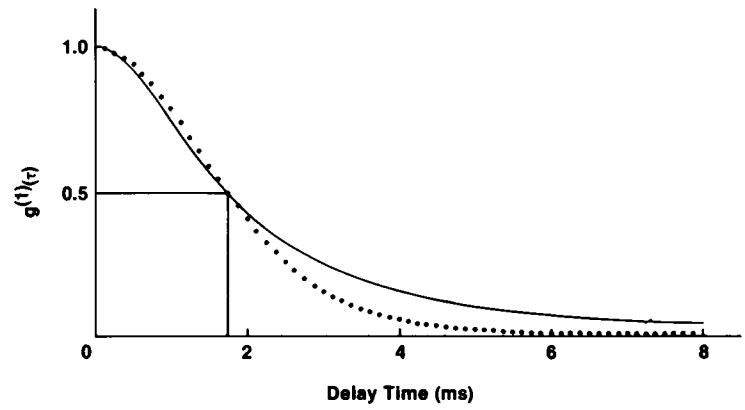

FIGURE 12 A comparison of f_N, a Lorentzian that represents the experimentally obtained scattering function (solid line) with a scattering function calculated with an equation equivalent to Eq. 18, but using normal distributions for $P_s(v)$ and $P(\omega)$. (a = 0.5 μm, b = 2.3 μm, c = 8.3 μm, α = 57°, β = 12°, $\bar{f}$ = 10 Hz.) This function is unaffected by the magnitude of $\bar{v}$.

distribution for $P(\omega)$ leads to the function illustrated in Fig. 12. All the parameters except c were fixed at the same values as before. The magnitude of c was then adjusted until the half-widths of the function matched that of f_N. This occurred when c had a value of 8.3 μm, which is fairly close to the value of 9.0 μm obtained using the exponential distributions. The shape of the curve, however, differs markedly from f_N.

CONCLUSIONS

By modeling bull spermatozoa as ellipsoidal Rayleigh-Gans-Debye particles whose semiaxes are similar to those of real cells, electric field autocorrelation functions can be calculated. These functions agree well with ones obtained experimentally. Parameters characterizing the detailed trajectory of the swimmer and the proper distribution functions for translational velocities and rotational frequencies are required for this calculation. So far only small scattering angles (15°) have been investigated. At higher angles it may be necessary to treat the scatterers as coated ellipsoids, or some other more complicated structure. While these calculations are underway they are quite lengthy, involving many hours of processing time on an Amdahl V/5 (Amdahl Corp., Sunnyvale, Calif.). However, preliminary evidence does indicate that the half-widths of the calculated functions, like the experimental functions, scale inversely with k for scattering angles less than 30°. In addition it is clear that either calculated or experimental functions from normal swimming cells can be fit very well by a simple Lorentzian function. Since a Lorentzian function results from the Fourier transform of a

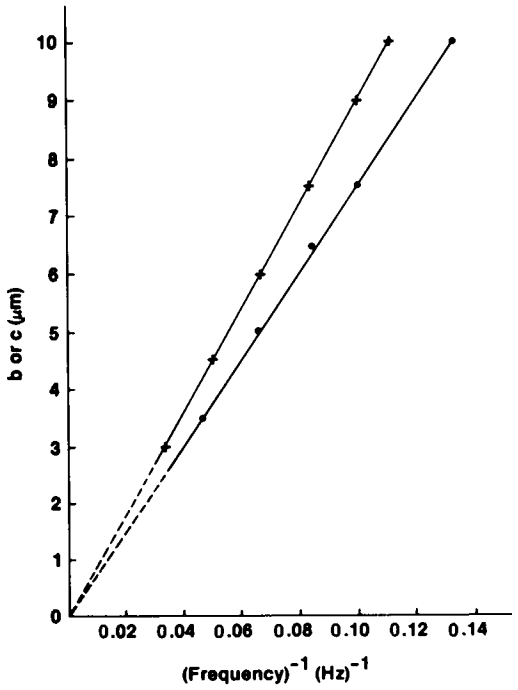

FIGURE 13 A graph of c (crosses) or $b = c$ for disks (dots) vs. the inverse of the average frequency that yields (using Eq. 18) functions of half-width 1.68 ms. $a = 5.0$ μm, $b = 2.3$ μm (ellipsoids), $\alpha = 57°$, $\beta = 12°$, $\bar{v} = 110$ μm s^{-1}.

distribution function such as Eq. 15 or 17, then the integrals in Eqs. 18 and 20 essentially perform this same operation. Lastly, we have shown that the half-widths of the scattering functions are determined primarily by the average rotational frequency of the cells and not by their translational velocity as previously believed. In these circumstances the half-width scales inversely with $\bar{\omega}$. These results imply that at low scattering angles experimental functions could be fit by a Lorentzian whose half-width scales inversely with $\bar{\omega}$ and k. Further evidence was obtained from the observation that many combinations of c and $\bar{\omega}$ yield functions of identical half-width. A similar result was obtained for disks. If the values of c (or b for disks) and $1/\bar{f} = 2\pi/\bar{\omega}$ are plotted against each other (Fig. 13), one obtains a straight line relationship. The only exception occurs when c (or b) becomes sufficiently small that the translational motion of the cells begins to alter the functions (dotted region). At low angles, therefore, it appears that the scattering function can be approximated by a Lorentzian having the form

$$f'_N = \frac{1}{1 + (Ck\bar{\omega}\tau)^2}, \tag{22}$$

where C is a constant determined by the shape of the scatterer and its orientation with respect to its axis of rotation. Again it should be emphasized that Eq. 22 applies only in the case where the rotating scatterer is sufficiently large and nonspherical that translational motion can be neglected.

Once values of C are known for any swimmer, then $\bar{\omega}$ would be routinely determined from least-squares fits or half-width determinations. For bull spermatozoa, C has a value of ~2.75 μm. Referring to arguments presented in the introduction, one may show that $C \simeq \ell/2\pi$, where ℓ is a linear dimension of the scatterer. Values of ℓ thus obtained are consistent with the dimensions of the ellipsoid used earlier to model spermatozoa.

We would like to thank Dr. P. A. Egelstaff for allowing us extensive use of his Nova 3 minicomputer and Dr. J. R. MacDonald for his encouragement and support.

This research was supported by a grant from the National Research Council of Canada.

Received for publication 21 May 1979 and in revised form 1 September 1979.

REFERENCES

ADAM, M., A. HAMELIN, P. BERGÉ, and M. GOFFAUX. 1969. Possibilité d'application de la technique de diffusion inélastique de la lumière à l'étude de la vitalité des spermatozoïdes de taureaux. *Ann. Biol. Anim. Biochim. Biophys.* **9**:651–655.

CHEN, S.-H., M. HOLZ, and P. TARTAGLIA. 1977. Quasi-elastic light scattering from structured particles. *Appl. Opt.* **16**:187–194.

COOKE, D., F. R. HALLETT, and C. A. V. BARKER. 1976. Motility evaluation of bull spermatozoa by photon correlation spectroscopy. *J. Mechanochem. Cell Motil.* **3**:219–223.

DUBOIS, M., P. JOUANNET, P. BERGÉ, B. VOLOCHINE, C. SERRES, and G. DAVID. 1975. Méthode et appareillage de mesure objective de la mobilité des spermatozoïdes humains. *Ann. Phys. Biol. Med.* **9**:19–41.

HALLETT, F. R., T. CRAIG, and J. MARSH. 1978. Swimming speed distributions of bull spermatozoa as determined by quasi-elastic light scattering. *Biophys. J.* **21**:203–216.

HOLZ, M., and S.-H. CHEN. 1978*a*. Structural effects in quasi-elastic light scattering from motile bacteria of *E. coli*. *Appl. Opt.* **17**:1930–1937.

HOLZ, M., and S.-H. CHEN. 1978*b*. Rotational-translational models for interpretation of quasi-elastic light scattering spectra of motile bacteria. *Appl. Opt.* **17**:3197–3204.

JOUANNET, P., B. VOLOCHINE, P. DEGUENT, C. SERRES, and G. DAVID. 1977. Light scattering determination of various characteristic parameters of spermatozoa motility in a serie of human sperm. *Andrologia.* **9**:36–49.

NOSSAL, R. 1971. Spectral analysis of laser light scattered from motile microorganisms. *Biophys. J.* **4**:341–354.

RIKMENSPOEL, R., G. VAN HERPEN, and J. EIJKHOUT. 1960. Cinematographic observations of the movement of bull sperm cells. *Phys. Med. Biol.* **5**:167–181.

SHIMIZU, H., and G. MATSUMOTO. 1977. Light scattering on motile spermatozoa. *(I.E.E.E.) Inst. Electr. Electron. Eng. Trans. Biomed. Eng.* **24**:153–157.

VAN DUIJN, JR. C., and C. VAN VOORST. 1971. Precision measurements of dimensions, refractive index and mass of bull spermatozoa in the living state. *Mikroskopie.* **27**:142–167.